Available online at www.sciencedirect.com
ScienceDirect
European Journal of Medicinal Chemistry 43 (2008) 2361–2372
EUROPEAN JOURNAL OF MEDICINAL CHEMISTRY
http://www.elsevier.com/locate/ejmech

Original article

3D and quantum QSAR of non-benzodiazepine compounds

F.A. Pasha [a], M. Muddassar [a], Seung Joo Cho [a,*], Kaleem Ahmad [b], Yakub Beg [c]

[a] *Computational Science Center, Korea Institute of Science and Technology, P.O. Box 131, Cheongryang, Seoul 130-650, Republic of Korea*
[b] *Department of Chemistry, M.L.K. (P.G.) College, Balrampur, Uttar Pradesh, India*
[c] *Department of Chemistry, Bareilly College, Bareilly, Uttar Pradesh, India*

Received 14 August 2007; received in revised form 19 December 2007; accepted 10 January 2008
Available online 2 February 2008

Abstracts

A combined physicochemical and 3D technique is used to establish the QSAR of four series of non-benzodiazepines towards BzR. In physicochemical QSAR study, the semi-empirical PM3 based parameters like hardness, electronegativity, electrophilicity index, molar refractivity, heat of formation, solvent assessable surface area and log *P* were used as descriptors. The heat of formation (HF) and log *P* are recognized as the most important descriptors for binding affinity of such compounds to BzR. The 3D QSAR study reveals that β-Carbolines of series ''A'' and Imidazo[1, 2-α]pyrimidines of series ''C'' show steric bulk interaction, the β-Carbolines of series ''B'' and di-substituted purines of series ''D'' have dominance of electrostatic interaction with BzR. The CoMSIA also indicate the same trend in terms of steric and electrostatic interaction. The CoMSIA reveals that only in case of series ''D'', the hydrophobic field effect is important. Some possible candidates for all four series were designed and their probable activities were estimated by using different QSAR models. The activities of designed molecules are in better range and developed models might be helpful to design the potent ligands of BzR.

Keywords: QSAR; Quantum chemical descriptors; CoMFA; CoMSIA; 3D QSAR

1. Introduction

Benzodiazepines are the drugs related to anxiety and emotional disorders. They act via the benzodiazepine receptor site (BzR) on the Gamma-amino butyric acid receptor ($GABA_A$) family and have been subjected to extensive QSAR studies [1–4]. Previously, a number of QSAR studies on classical benzodiazepine molecules have been reported [2–5]. The several non-benzodiazepine compounds like β-Carbolines, Imidazo[1, 2-α]pyrimidines, di-substituted purines also binds with BzR with a high affinity. Thus, all compounds that bind to the BzR should have certain common characteristics that allow for recognition by the receptor regardless of the type of (in vivo) activity. Molecular modeling studies have determined that all BDZ ligands share the presence of an aromatic or heteroaromatic ring, believed to undergo π/π stacking with aromatic amino acid residues within the receptor, as well as a proton-accepting group that exists in the same plane of the aromatic ring and interacts with a histidine residue on the receptor [4]. The structural diversity among non-benzodiazepine compounds makes it difficult to generalize the molecular requirements for BzR. The QSAR and computational techniques are the prominent tools to explore the relationship between structures of ligands with their binding affinities. Different methods like physical and electronic properties based QSAR and 3D QSAR [6] are in practice [7–10]. In the present study, we have taken four series of non-benzodiazepine compounds with their observed binding affinities [11–20]. The different QSAR models were developed to establish a generalized relation for heterogeneous data set of non-benzodiazepine derivatives. Since the drug molecules are active only when they have certain physicochemical properties with specific 3D structure in this way the physicochemical and three-dimensional aspects have equal importance for a molecule to be a medicine. The current study

* Corresponding author.
E-mail addresses: fpasha@rediffmail.com (F.A. Pasha), chosj@kist.re.kr (S.J. Cho).

0223-5234/$ - see front matter © 2008 Published by Elsevier Masson SAS.
doi:10.1016/j.ejmech.2008.01.030

deals the physicochemical QSAR as well as 3D aspects by comparative molecular field analysis (CoMFA) and comparative molecular similarity analysis (CoMSIA).

2. The study material

Four different series (namely A, B, C and D) of non-benzodiazepine compounds were taken with their observed affinities to BzR.

2.1. Series A

The parent skeleton of series "A" is given in Fig. 1 and Table 1 contains 23 such β-Carbolines with their observed affinities [11–14].

2.2. Series B

The β-Carbolines also posses a broad spectrum of pharmacological actions mediated via occupation of BzR in the central nervous system. The parent skeleton of series "B" is given in Fig. 2 and Table 2 contains 17 such β-Carbolines with their observed affinities [14–16].

2.3. Series C

The parent skeleton of series "C" is given in Fig. 3. This series contains 20 derivatives of Imidazo[1, 2-α]pyrimidine with their observed affinities [17] as reported in Table 3. The Imidazo[1, 2-α]pyrimidines inhibit the binding of [^{3}H] flunitrazepam from rat brain preparations.

2.4. Series D

The parent skeleton of series "D" is given in Fig. 4. Table 4 contains 31 derivatives of 6,9 di-substituted purines with their observed binding affinities to the rat brain tissue [18–20].

3. Computational method

3.1. The physicochemical QSAR

The physicochemical parameter based QSAR study was performed by the following important descriptors like partition function (log *P*) [21], molar refractivity (MR) [22], solvent assessable surface area (SASA) [22], dielectric energy (DE) [22], global hardness (η) [23], electronegativity (χ) [24], electrophilicity index (ω) [25], and connectivity index (order 0, standard) (CI) [22]. The molecules were drawn by CAChe pro software and the geometries were optimized at PM3 level in conjunction with molecular mechanics. The log *P*, MR, SASA and DE values of every molecule were calculated by project leader software associated with CAChe pro. The global hardness and electronegativities were calculated using frontier orbital energies obtained from PM3 results and reported in Tables 5–8. Multiple linear regression analysis (MLR) is performed to establish the QSAR. Some molecules of different sets not predicted well in initial step of regression were omitted from final model and reported as outliers.

Table 1
β-Carbolines of series "A" and their observed biological activities (pIC_{50}) [11–14]

Comp. no.	R1	R2	pIC_{50}
1	H	$COOCH_3$	8.3
2	H	$COOC_2H_5$	8.3
3	H	OC_2H_5	7.62
4	H	$OCH(CH_3)_2$	6.29
5	H	OC_4H_9	7.01
6	H	OCH_3	6.91
7	H	OC_3H_7	7.96
8	H	COC_3H_7	7.64
9	H	C_4H_9	6.64
10	H	H	5.79
11	H	$COOC(CH_3)_3$	8
12	H	Cl	7.35
13	H	NO_2	6.9
14	H	$COOCH_2C(CH_3)_3$	6.12
15	C_2H_5	$COOCH_3$	5.12
16	C_2H_5	H	3.6
17	CH_3	H	4.91
18	$OCH(CH_3)CH_2CH_3$	H	6.33
19	$OCH_2CH(CH_3)_2$	H	7.03
20	$OCH_2CH_2CH(CH_3)_2$	H	6.27
21	$OCH_2C(CH_3)_3$	H	7.02
22	$OCH_2C_6H_5$	H	6
23	$COC(CH_3)_3$	H	6.45

The $pIC_{50} = -\log IC_{50}$ and the IC_{50} values are the molar concentration of inhibitor that produces 50% inhibition of [^{3}H] diazepam binding to rat brain benzodiazepine receptors.

3.2. Multiple linear regression (MLR) analysis

MLR analyses were performed using SPSS software. The quantum mechanical descriptors were used as independent variables and the pIC_{50} values as the dependent variables. In the statistical analyses, the systematic search was performed to determine the significant descriptors. The correlation matrix was developed to minimize the effect of co-linearity and to avoid redundancy and the variables physically removed from the analysis, which shows exact linear dependencies between subsets of

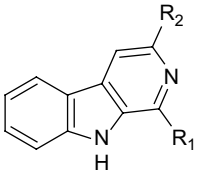

Fig. 1. The parent structure of β-Carbolines for series "A".

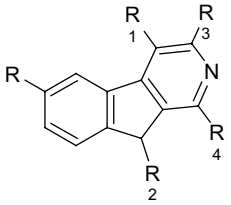

Fig. 2. The parent structure of β-Carbolines for series "B".

Table 2
β-Carbolines of series "B" and their observed biological activities (pIC_{50}) [14–16]

Comp. no.	R	R1	R2	R3	pIC_{50}
1	H	H	H	Cl	7.35
2	H	H	H	NO_2	6.9
3	H	H	H	NCS	8.1
4	H	H	H	$COOCH_3$	8.3
5	H	H	H	H	5.79
6	H	H	H	OCH_3	6.91
7	H	H	H	$OC2H_5$	7.62
8	H	H	H	$OC3H_7$	7.96
9	H	H	H	NH_2	4.6
10	H	H	H	OH	5.4
11	$OCH_2C_6H_5$	CH_2OCH_3	H	$COOC_2H_5$	9
12	OH	CH_2OCH_3	H	$COOC_2H_5$	9.05
13	$OCH_2C_6H_5$	CH_2OCH_3	CH_3	$COOC_2H_5$	6.02
14	OCH_3	CH2OCH3	H	$COOC_2H_5$	9.3
15	H	CH2OCH3	H	$COOC_2H_5$	8.64
16	$OCH_2C_6H_5$	C_2H_5	H	$COOC_2H_5$	7.66
17	$OCH_2C_6H_5$	H	H	$COOC_2H_5$	8.05

The $pIC_{50} = -\log IC_{50}$ and the IC_{50} values are the molar concentration of inhibitor that produces 50% inhibition of [^{3}H] diazepam binding to the benzodiazepine receptors.

Table 3
Imidazo[1, 2-α]pyrimidines of series "C" and their observed biological activities (pIC_{50}) [17]

Comp. no.	R1	R2	R3	pIC_{50}
1	CH_3	$CH_2CH{=}CH_2$	SCH_3	8.097
2	CH_3	CH_2CH_3	SCH_3	7.921
3	CH_3	$CH_2CH{=}CCH_2$	OCH_3	7.523
4	CH_2CH_3	$CH_2CH_2CH_3$	OCH_3	7.469
5	CH_2CH_3	$CH_2CH_2CH_2CH_3$	OCH_3	7.469
6	CH_3	$CH_2CH_2CH_2CH_3$	OCH_3	7.377
7	CH_2CH_3	$CH_2CH{=}CCH_2$	OCH_3	7.377
8	CH_3	$CH_2CH{=}CCH_2$	OCH_3	7.347
9	CH_2CH_3	$CH_2CH_2CH_3$	SCH_3	7.328
10	CH_3	CH_2CH_3	OCH_3	7.252
11	CH_3	$CH_2CH_2CH_3$	OCH_3	7.071
12	$CH_2CH_2CH_3$	H	SCH_3	7.051
13	CH_2CH_3	CH_2CH_3	OCH_3	6.971
14	CH_3	H	SCH_3	6.721
15	CH_2CH_3	H	OCH_3	6.53
16	$CH_2CH_2CH_2CH_3$	H	OCH_3	6.469
17	$CH_2CH_2CH_3$	H	OCH_3	6.272
18	CH_3	H	OCH_3	6.097
19	CH_3	OCH_3	OCH_3	6
20	H	CH_2CH_3	OCH_3	5.824

The $pIC_{50} = -\log IC_{50}$ and the IC_{50} values are the molar concentration of inhibitor that produces 50% inhibition of specific binding of 0.6 nM [^{3}H] flunitrazepam to rat forebrain membrane.

the variables and multi-co-linearity (high multiple correlations between subsets of the variables). In order to explore the reliability of the proposed model, we used the cross-validation method. Prediction error sum of squares (PRESS) is a standard index to measure the accuracy of a modeling method based on the cross-validation technique. The r^2_{cv} is calculated by using Eq. (1) based on the PRESS and SSY (sum of squares of deviations of the experimental values from their mean).

$$r^2_{cv} = 1 - \frac{\text{PRESS}}{\text{SSY}} = 1 - \frac{\sum_{i=1}^{n}\left(y_{exp} - y_{pred}\right)^2}{\sum_{i=1}^{n}\left(y_{exp} - \bar{y}\right)^2} \quad (1)$$

3.3. 3D QSAR

In 3D QSAR study structures were minimized at Tripos force field [26] level and Gasteiger–Huckel charges with a distance-dependent dielectric and conjugate gradient method by using SYBYL 7.3 [27] software. The convergence criterion was 0.01 kcal mol^{-1}. These structures were used for 3D quantitative structure–activity relationship (3D QSAR), the comparative molecular field analysis (CoMFA) and comparative molecular similarity indices analysis (CoMSIA) [6,28].

3.4. The molecular alignment

CoMFA and CoMSIA require the alignment of 3D structures according to a suitable conformational template, which is assumed to be a bioactive conformation [6]. The systematic search based minimum energy conformer of most active molecule of each series was taken as template. The template was modified for further ligands by fixing common moiety and the molecules were aligned (Figs. 5–8) on corresponding templates by using common substructure.

3.5. The CoMFA and CoMSIA

Lennard-Jones and Coulomb potentials [29] based CoMFA analysis has been performed and the steric as well as electrostatic energies were calculated by using a sp^3 carbon probe atom with Van der Waals radius of 1.52 Å and a +1 charge. The energies were truncated to ±30 kcal mol^{-1} and the electrostatic contributions were ignored at lattice interactions with maximum steric interactions. The CoMFA was generated by standard method in SYBYL. The CoMSIA models were also derived with the same lattice box used as in CoMFA calculations. CoMSIA similarity indices (steric, electrostatic and hydrophobic) were evaluated using the probe atom. The CoMSIA model from hydrophobic field was calculated between the grid point and each atom of the molecule by a Gaussian distance function [30]. The attenuation factor's default value of 0.30 was used,

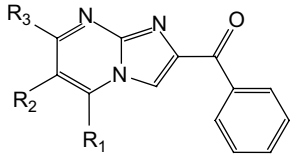

Fig. 3. Parent structure of Imidazo[1, 2-α]pyrimidines for series "C".

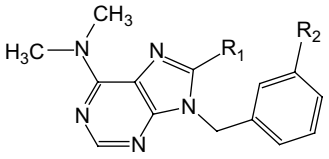

Fig. 4. The parent structure of di-substituted purines for series "D".

Table 4
Di-substituted purines of series "D" and their observed biological activities (pIC_{50}) [18–20]

Comp. no.	R1	R2	pIC_{50}
1	H	H	4.89
2	Br	H	5.52
3	CH_3	H	5.07
4	OCH_3	H	5.27
5	$N(CH_3)_2$	H	5.24
6	$NHCH_3$	H	4.77
7	H	3-NH_2	6.05
8	Br	3-NH_2	6.96
9	Cl	3-NH_2	6.72
10	OCH_3	3-NH_2	6
11	$N(CH_3)_2$	3-NH_2	6.22
12	$NHCH_3$	3-NH_2	5.14
13	OH	3-NH_2	5.74
14	H	3-NHCHO	7.47
15	Br	3-NHCHO	7.96
16	$N(CH_3)_2$	3-NHCHO	6.96
17	$NHCH_3$	3-NHCHO	6.44
18	OH	3-NHCHO	6.89
19	Br	3-$NHCOCH_3$	6.08
20	Br	3-$NHCOC_6H_5$	5.1
21	Br	3-$NHCOOCH_3$	5.28
22	Br	3-$NHCONH_2$	7.6
23	Br	3-$NHSO_2CH_3$	5.82
24	H	3-F	5.14
25	H	3-CH_2OH	5.3
26	H	3-OH	5.92
27	H	3-$OCOC(CH_3)_3$	5.8
28	H	3-$OCOCH_3$	6.36
29	H	2-F	5.27
30	H	2-Cl	4.89
31	H	2-OCH_3	4.7

The $pIC_{50} = -\log IC_{50}$ and the IC_{50} values are the molar concentration of inhibitor that produces 50% inhibition of [^{3}H] diazepam binding to rat brain benzodiazepine receptors.

which is the standard distance dependence of molecular similarity. The effect of using the standard attenuation factor is shown in contour maps with prominent molecular features.

3.6. Partial least square (PLS) analysis and validation of QSAR models

To derive 3D QSAR models, the CoMFA and CoMSIA descriptors were used as independent variables and the pIC_{50} values as the dependent variables. PLS method [31,32] was used to linearly correlate these CoMFA and CoMSIA descriptors to the activity. The CoMFA cutoff values were set to 30 kcal mol^{-1} for both steric and electrostatic fields, and all fields were scaled by the default options in SYBYL. The cross-validation analysis was performed using the leave one out (LOO) method in which one compound is removed from the data set and its activity is predicted using the model derived from the rest of the data set. The cross-validated correlation coefficient (q^2) that resulted in optimum number of components and lowest standard error of prediction were considered for further analysis and calculated using the following equation:

Table 5
Values of descriptors with observed and predicted biological activities of series "A"

Comp. no.	Log *P*	HF	η	SASA	pIC_{50}	PA_A
1	1.404	−18.288	3.987	111.24	8.3	8.56
2	1.746	−24.944	4.051	119.716	8.3	7.712
3	2.063	16.692	3.925	108.645	7.62	7.446
4	2.476	11.383	3.924	114.618	6.29	7.136
5	2.928	6.041	3.925	123.399	7.01	6.955
6	1.72	21.332	3.93	100.467	6.91	7.361
7	2.531	11.445	3.925	116.107	7.96	7.128
8	2.006	11.192	3.972	119.644	7.64	7.869
9[a]	3.185	36.699	4.033	117.486	6.64	4.029
10	1.274	62.277	3.976	88.615	5.79	6.197
11	2.237	−33.773	4.053	130.22	8	7.625
12	2.163	55.119	3.91	100.12	7.35	6.286
13	1.927	54.031	3.944	101.892	6.9	6.469
14	3.123	−39.55	4.051	135.551	6.12	6.278
15[a]	2.522	−32.887	4.033	124.554	5.12	6.816
16	2.392	47.929	4.035	101.357	3.6	4.218
17	1.924	52.362	4.03	94.946	4.91	4.69
18	3.33	1.577	3.924	128.322	6.33	6.578
19	2.934	6.395	3.924	121.999	7.03	6.836
20	3.258	0.581	3.925	128.75	6.27	6.771
21	3.44	1.589	3.923	126.467	7.02	6.204
22	3.497	50.869	3.925	134.326	6	6.156
23	2.554	8.113	3.925	118.507	6.45	7.324

[a] Data point not used in deriving model.

$$q^2 = 1 - \frac{\sum_y \left(y_{\text{pred}} - y_{\text{observed}}\right)^2}{\sum_y \left(y_{\text{observed}} - y_{\text{mean}}\right)^2} \quad (2)$$

where, γ_{pred}, γ_{actual} and γ_{mean} are predicted, actual, and mean values of the target property (pIC_{50}), respectively, and PRESS is the sum of predictive sum of squares. The non-cross-validated PLS analyses were performed with a column filter value of 2.0, to reduce analysis time with small effect on the q^2

Table 6
Values of descriptors with observed and predicted biological activities of series "B"

Comp. no.	HF	CI	μ	pIC_{50}	PA_B
1	55.119	9.544	−4.526	7.35	6.341
2	54.031	11.121	−5.156	6.9	7.268
3[a]	103.516	10.958	−4.606	8.1	5.676
4	−19.584	11.828	−4.833	8.3	8.009
5	62.277	8.673	−4.446	5.79	6.104
6	21.332	10.251	−4.542	6.91	6.917
7	18.126	10.958	−4.322	7.62	6.661
8	12.875	11.665	−4.325	7.96	6.754
9	62.726	9.544	−3.974	4.6	5.428
10	14.673	9.544	−4.382	5.4	6.792
11	−72.315	20.217	−4.683	9	8.709
12	−109.216	15.69	−4.723	9.05	9.335
13[a]	−73.453	21.087	−4.633	6.02	8.661
14	−102.142	16.397	−4.692	9.3	9.181
15	−64.588	14.82	−4.792	8.64	8.702
16	−44.57	19.51	−4.681	7.66	8.249
17	−33.8	17.933	−4.691	8.05	8.078

[a] Data point not used in deriving model.

Table 7
Values of descriptors with observed and predicted biological activities of series "C"

Comp. no.	Log *P*	HF	SASA	pIC_{50}	PA_C
1	2.704	64.798	153.128	8.097	8.053
2	2.523	39.733	146.891	7.921	7.328
3	2.402	25.735	151.519	7.523	7.455
4	3.045	−9.665	152.958	7.469	7.088
5	3.441	−18.057	160.678	7.469	7.481
6	2.972	−6.196	155.207	7.377	7.281
7	2.829	19.65	150.799	7.377	7.323
8	2.361	23.966	147.958	7.347	7.199
9[a]	3.388	34.295	159.882	7.328	8.096
10[a]	2.18	4.574	140.378	7.252	6.458
11	2.576	−0.785	147.62	7.071	6.859
12	2.714	40.447	151.627	7.051	7.644
13	2.648	−2.316	145.432	6.971	6.695
14	1.849	50.077	138.037	6.721	6.89
15	1.974	6.941	136.898	6.53	6.264
16	2.767	−4.13	151.576	6.469	7.073
17	2.37	1.314	144.265	6.272	6.669
18	1.506	10.43	130.633	6.097	5.905
19	0.637	−22.644	139.925	6	6.106
20	2.617	8.3	136.92	5.824	6.273

[a] Data point not used in deriving model.

values. To further assess the robustness and statistical confidence of the derived models, bootstrapping analysis for 10 runs was performed.

To assess the predictive power of the 3D QSAR models derived using the training sets, activity of test sets was predicted. The predictive ability of the models is expressed by the predictive r^2 value, which is analogous to cross-validated $r^2(q^2)$ and is calculated using the following equation:

$$r^2_{\text{pred}} = \frac{\text{SD} - \text{PRESS}}{\text{SD}} \tag{3}$$

$$\text{PRESS} = \sum_{y} \left(y_{\text{predicted}} - y_{\text{observed}}\right)^2 \tag{4}$$

where SD is the sum of the squared deviations between the biological activities of the test set and the mean activities of the training molecules and PRESS is the sum of squared deviation between the predicted and the observed activity of the test sets and is calculated using Eq. (4).

4. Results

The physicochemical QSAR study was performed by different descriptors. The MLR analyses were employed and the best model was identified by coefficient (r^2) and (r^2_{cv}) values. Predicted activities (PA) of series A, B, C and D are reported as PA_A, PA_B, PA_C and PA_D. In case of series A, the log *P*, heat of formation (HF), hardness (η) and solvent accessibility surface area (Å^2) (SASA) jointly give good correlation ($r^2_{\text{cv}} = 0.71$, $r^2 = 0.77$) as clear from the following equation:

Table 8
Values of descriptors with observed and predicted biological activities of series "D"

Comp. no.	Log *P*	CI	μ	pIC_{50}	PA_4
1	2.706	13.242	−4.418	4.89	5.426
2	4.106	14.113	−4.711	5.52	5.623
3	3.303	14.113	−4.379	5.07	4.951
4	3.363	14.82	−4.341	5.27	4.899
5	3.88	15.69	−4.427	5.24	5
6	3.19	14.82	−4.291	4.77	4.842
7	1.923	14.113	−4.379	6.05	6.116
8	3.323	14.983	−4.722	6.96	6.516
9	3.023	14.983	−4.511	6.72	5.912
10	2.58	15.69	−4.302	6	5.589
11	3.097	16.56	−4.432	6.22	5.869
12	2.406	15.69	−4.289	5.14	5.683
13	2.548	14.983	−4.337	5.74	5.606
14	1.84	15.527	−4.519	7.47	7.061
15	3.24	16.397	−4.845	7.96	7.391
16	3.014	17.974	−4.419	6.96	6.191
17	2.323	17.104	−4.454	6.44	6.729
18	2.465	16.397	−4.476	6.89	6.546
19	2.955	17.267	−4.542	6.08	6.588
20	4.868	20.38	−4.555	5.1	5.698
21[a]	3.581	17.974	−4.644	5.28	6.626
22	2.684	17.267	−4.551	7.6	6.854
23	2.873	18.19	−4.659	5.82	7.332
24	2.846	14.113	−4.518	5.14	5.902
25[a]	2.171	14.82	−4.446	5.3	6.331
26	2.422	14.113	−4.45	5.92	5.984
27	5.461	19.767	−4.687	5.8	5.602
28	3.605	17.267	−4.593	6.36	6.247
29	2.846	14.113	−4.488	5.27	5.78
30	3.224	14.113	−4.462	4.89	5.355
31[a]	2.453	14.82	−4.433	4.7	6.040

[a] Data point not used in deriving model. CI = connectivity index (order 0, standard).

$$\begin{aligned} PA_A = {} & -2.121 \times \log P - 0.011 \times \text{HF} - 14.251 \\ & \times \eta + 0.083 \times \text{SASA} + 58.884 \\ & r^2_{\text{cv}} = 0.71,\ r^2 = 0.77 \end{aligned} \tag{5}$$

The compounds **9** and **15** are omitted from the final model but the activities and descriptors values are within normal range and they don't have any unusual subsistent. Though these compounds can be included in other model but unfortunately we cannot adopt those models due to co-linearity of descriptors. These compounds are outliers probably due to some topological factors.

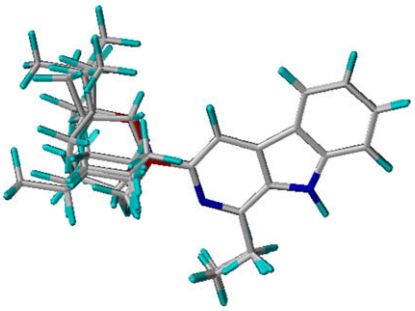

Fig. 5. The aligned structures of series "A".

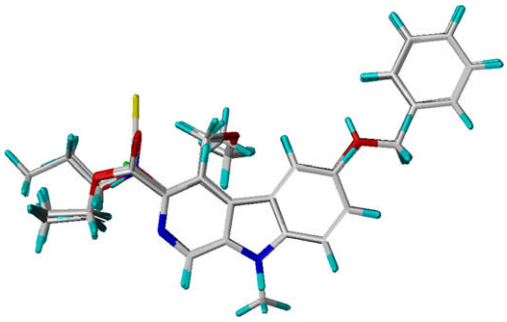

Fig. 6. The aligned structures of series "B".

The negative coefficient of log P and hardness indicates that hydrophobic and electronic interaction is not significantly contributes to activity but the positive coefficient of SASA indicates the contribution of bulkiness to activity which is in consonance with earlier study [4]. Similarly the HF, connectivity index (order 0, standard) (CI) and chemical potential (μ) give good correlation ($r^2_{cv} = 0.60$, $r^2 = 0.74$) for series "B" as clear from the following equation:

$$PA_B = -0.0163 \times HF + 0.007 \times CI - 1.428 \times \mu + 0.708$$
$$r^2_{cv} = 0.60,\ r^2 = 0.74 \quad (6)$$

The compounds **3** and **13** were omitted from model. As clear from data, the chain elongation with bulk at site R3 is favorable for activity but the compound **3** holds a sulfur (bulk) atom without chain elongation. Similarly, all compounds of series hold hydrogen atom at site R2 but the compound **13** holds a hydrophobic methyl group at site R2. Probably due to these factors, the compounds **3** and **13** are outlier.

The best-fitted model of series "C" is obtained by log P, HF and SASA. The regression equation (7) has been generated by these descriptors and gives high correlation ($r^2_{cv} = 0.22$, $r^2 = 0.75$).

$$PA_C = -0.015 \times \log P + 0.013 \times HF + 0.065 \times SASA - 2.761$$
$$r^2_{cv} = 0.22,\ r^2 = 0.75 \quad (7)$$

The compounds **9** and **10** were not included in model, however, these compounds are usually subsistent and the values of global descriptors like log P, HF and SASA are in normal range. These compounds are outliers probably due to some topological factors.

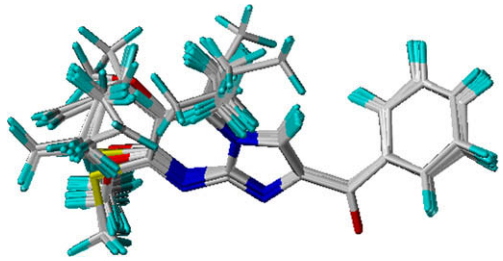

Fig. 7. The aligned structures of series "C".

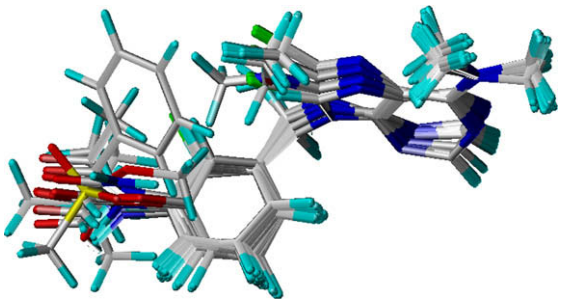

Fig. 8. The aligned structures of series "D".

Similarly for series "D", the best-fitted model is obtained by log P, CI, and chemical potential as clear from the following equation:

$$PA_D = -0.844 \times \log P + 0.216 \times CI - 4.065 \times \mu - 13.105$$
$$r^2_{cv} = 0.46,\ r^2 = 0.63 \quad (8)$$

The compounds **21**, **25** and **31** were not included in model. Litina et al. explain that site R2 makes contact with hydrophobic pocket. Only compounds **21** and **31** have OCH3 terminal at R2 which is quite a hydrophobic group and probably due to this group they are outliers but the compound **25** does not contain any unusual group and the reason is still unclear which makes it outlier. A close look at data reveals that heat of formation and log P are the most important descriptors. The best-fitted models of series "A" and "C" are based on log P, HF, and SASA. This finding indicates that, compounds of both these series have similar interaction with their targets. The best-fitted model of series "B" and "D" is based on chemical potential and connectivity index, which indicates the dominance of electrostatic interaction. In short, the series "A" and "C" show quite resemblance and have similar steric bulk interaction while series "B" and "D" have electrostatic interaction. In order to have more generalized model and to validate the findings the 3D QSAR analyses were performed.

4.1. 3D QSAR study

In 3D QSAR, the CoMFA and CoMSIA studies were performed. Each series were divided into training and test sets as given in Tables 9–12.

4.2. CoMFA model

3D QSAR analyses were conducted by correlating the biological activities of the different compound with CoMFA fields using the partial least-squares (PLS) method. All four series of compounds were divided into training and test sets. The steric and electrostatic fields effect, individually and in combinations, were tested. The compounds of series "A" showed strong correlation with steric field effects. The best-fitted model $CoMFA_1$ of series "A" has the values of $q^2 = 0.57$, $r^2 = 1.00$ with $r^2_{predictive} = 0.61$. Similarly for series "B", a strong correlation appears with electrostatic field effects. The best-fitted model $CoMFA_2$ of series "B" has the values of $q^2 = 0.81$, $r^2 = 0.98$

Table 9
The observed activity and predicted activity by CoMFA and CoMSIA models with residual values for series A

Comp. no.	Observed pIC_{50}	$CoMFA_1$		$CoMSIA_1$	
		$pIC_{50\ predicted}$	Resid.	$pIC_{50\ predicted}$	Resid.
1	8.3	8.299	0.001	8.312	−0.012
2	8.3	8.29	0.01	8.369	−0.069
3	7.62	7.622	−0.002	7.537	0.083
5	7.01	7.019	−0.009	7.017	−0.007
7	7.96	7.958	0.002	7.9	0.06
8	7.64	7.647	−0.007	7.525	0.115
9	6.64	6.639	0.001	6.61	0.03
11	8	8.006	−0.006	8.044	−0.044
12	7.35	7.347	0.003	7.275	0.075
13	6.9	6.899	0.001	6.962	−0.062
14	6.12	6.118	0.002	6.108	0.012
15	5.12	5.12	0	5.064	0.056
17	4.91	4.913	−0.003	5.012	−0.102
18	6.33	6.317	0.013	6.288	0.042
19	7.03	7.045	−0.015	7.23	−0.2
21	7.02	7.011	0.009	7.017	0.003
22	6	6.001	−0.001	5.979	0.021
Test set					
4	6.29	7.622	−1.332	6.994	−0.704
6	6.91	6.997	−0.087	7.531	−0.621
10	5.79	6.739	−0.949	7.119	−1.329
16	3.6	3.497	0.103	3.817	−0.217
20	6.27	7.131	−0.861	6.451	−0.181
23	6.45	7.283	−0.833	8.096	−1.646

with $r^2_{predictive} = 0.46$. The compounds of series "C" show significant relations with steric field effect and the best-fitted model ($CoMFA_1$) has the values of $q^2 = 0.57$, $r^2 = 0.98$ with $r^2_{predictive} = 0.47$. The compounds of series "D" show strong relationships with electrostatic field effects and the best-fitted model $CoMFA_2$ has the values of $q^2 = 0.66$, $r^2 = 0.97$ with $r^2_{predictive} = 0.63$. The results of CoMFA are summarized in

Table 10
The observed activity and predicted activity by CoMFA and CoMSIA models with residual values for series B

Comp. no.	Observed pIC_{50}	$CoMFA_2$		$CoMSIA_2$	
		$pIC_{50\ predicted}$	Resid.	$pIC_{50\ predicted}$	Resid.
1	7.35	7.024	0.326	7.438	−0.088
2	6.9	7.134	−0.234	6.9	0
3	8.1	8.102	−0.002	8.107	−0.007
4	8.3	8.299	0.001	8.286	0.014
5	5.79	6.033	−0.243	5.704	0.086
6	6.91	6.692	0.218	6.963	−0.053
7	7.62	7.701	−0.081	7.647	−0.027
8	7.96	7.96	0	7.842	0.118
10	5.4	5.354	0.046	5.435	−0.035
11	9	8.99	0.01	9.043	−0.043
12	9.05	9.077	−0.027	9.072	−0.022
13[a]	6.02	8.936	−2.916	8.726	−2.706
14	9.3	9.264	0.036	9.238	0.062
17	8.05	8.1	−0.05	8.055	−0.005
Test set					
9	4.6	5.736	−1.136	5.906	−1.306
15	8.64	9.162	−0.522	9.298	−0.658
16	7.66	9.561	−1.901	8.267	−0.607

[a] Data point not used in equation.

Table 11
The observed activity and predicted activity by CoMFA and CoMSIA models with residual values series C

Comp. no.	Observed pIC_{50}	$CoMFA_1$		$CoMSIA_1$	
		$pIC_{50\ predicted}$	Resid.	$pIC_{50\ predicted}$	Resid.
1	8.1	8.122	−0.022	8.137	−0.037
2	7.92	7.966	−0.046	7.955	−0.035
3	7.52	7.494	0.026	7.437	0.083
4	7.47	7.423	0.047	7.326	0.144
5	7.47	7.404	0.066	7.562	−0.092
6	7.38	7.452	−0.072	7.417	−0.037
9	7.33	7.33	0	7.279	0.051
10	7.25	7.023	0.227	7.094	0.156
11	7.07	7.119	−0.049	7.127	−0.057
12	7.05	7.08	−0.03	7.021	0.029
13	6.97	7.099	−0.129	7.13	−0.16
14	6.72	6.633	0.087	6.468	0.252
16	6.47	6.485	−0.015	6.38	0.09
17	6.27	6.23	0.04	6.41	−0.14
18	6.1	6.124	−0.024	6.331	−0.231
19	6	6.105	−0.105	6.014	−0.014
Test set					
7	7.38	7.404	−0.024	7.101	0.279
8	7.35	7.667	−0.317	7.528	−0.178
15	6.53	6.158	0.372	6.295	0.235
20	5.82	6.689	−0.869	6.116	−0.296

Table 12
The observed activity and predicted activity by CoMFA and CoMSIA models with residual values for series D

Comp. no.	Observed pIC_{50}	$CoMFA_2$		$CoMSIA_2$	
		$pIC_{50\ predicted}$	Resid.	$pIC_{50\ predicted}$	Resid.
1	4.89	5.133	−0.243	5.098	−0.208
2	5.52	5.197	0.323	5.459	0.061
3	5.07	4.839	0.231	5.158	−0.088
4	5.27	5.347	−0.077	5.166	0.104
5	5.24	5.268	−0.028	5.22	0.02
6	4.77	4.677	0.093	5.188	−0.418
7	6.05	5.94	0.11	5.7	0.35
10	6	5.971	0.029	5.8	0.2
11	6.22	6.022	0.198	5.489	0.731
12	5.14	5.378	−0.238	5.606	−0.466
13	5.74	5.9	−0.16	5.993	−0.253
15	7.96	7.982	−0.022	7.169	0.791
17	6.44	6.42	0.02	6.572	−0.132
19	6.08	6.085	−0.005	6.229	−0.149
20	5.1	5.121	−0.021	4.942	0.158
21	5.28	5.269	0.011	6.09	−0.81
22	7.6	7.589	0.011	7.474	0.126
23	5.82	5.78	0.04	6.602	−0.782
24	5.14	5.04	0.1	4.912	0.228
25	5.3	5.271	0.029	5.338	−0.038
26	5.92	5.844	0.076	5.238	0.682
27	5.8	5.694	0.106	5.75	0.05
28	6.36	6.469	−0.109	5.836	0.524
29	5.27	5.273	−0.003	5.109	0.161
30	4.89	5.189	−0.299	5.038	−0.148
31	4.7	4.869	−0.169	5.394	−0.694
Test set					
8	6.96	5.901	1.059	6.035	0.925
9	6.72	5.964	0.756	5.981	0.739
14	7.47	7.867	−0.397	6.816	0.654
16	6.96	6.245	0.715	6.082	0.878
18	6.89	7.137	−0.247	6.793	0.097

Table 13
The statistical summary of 3D QSAR models

Comp. no.	Analysis	Field	n	q^2	r^2	SE	F value	r^2_{bs}	SD	$r^2_{predictive}$
Series A										
1	$CoMFA_1$	Steric	10	0.57	1	0.01	126.86	1	0	0.61
1	$CoMFA_2$	Electrostatic	4	−0.09	–	–	–	–	–	–
2	$CoMSIA_1$	Steric	10	0.34	0.99	0.12	101.47	0.99	0.001	0.49
3	$CoMSIA_2$	Electrostatic	1	−0.23	–	–	–	–	–	–
4	$CoMSIA_3$	Hydrophobic	10	0.26	–	–	–	–	–	–
Series B										
1	$CoMFA_1$	Steric	6	0.71	–	–	–	–	–	–
1	$CoMFA_2$	Electrostatic	7	0.81	0.98	0.23	42.85	0.99	0.001	0.46
2	$CoMSIA_1$	Steric	5	0.68	–	–	–	–	–	–
3	$CoMSIA_2$	Electrostatic	7	0.94	0.99	.09	302.4	1	0	0.74
4	$CoMSIA_3$	Hydrophobic	8	0.21	–	–	–	–	–	–
Series C										
1	$CoMFA_1$	Steric	5	0.57	0.98	0.1	102.5	0.99	0.006	0.47
1	$CoMFA_2$	Electrostatic	1	−0.42	–	–	–	–	–	–
2	$CoMSIA_1$	Steric	5	0.72	0.96	0.15	44.93	0.98	0.02	0.87
3	$CoMSIA_2$	Electrostatic	1	0.027	–	–	–	–	–	–
4	$CoMSIA_3$	Hydrophobic	10	0.61	–	–	–	–	–	–
Series D										
1	$CoMFA_1$	Steric	3	0.07	–	–	–	–	–	–
1	$CoMFA_2$	Electrostatic	9	0.66	0.97	0.21	51.8	0.98	0.016	0.63
2	$CoMSIA_1$	Steric	1	−0.02	–	–	–	–	–	–
3	$CoMSIA_2$	Electrostatic	10	0.46	–	–	–	–	–	–
4	$CoMSIA_3$	Hydrophobic	3	0.47	0.72	0.45	18.5	0.77	0.11	0.6

Table 13. The predicted activities of training and test sets of all four series (A–D) are reported in Tables 9–12, respectively. The study indicates that binding affinities of series "A" and "C" have strong relation with steric field effects while dominance of electrostatic field effects to series "B" and "D".

4.3. The CoMFA contour map

The 3D-CoMFA maps of all four series with best-fitted model were shown in Figs. 9–12. The CoMFA green contour indicates the area in which steric bulk might have good effect over activity while yellow region favorable for small groups. The blue contour indicates the region where positive groups require for high activity while red zone indicates the place favorable for negative groups (for interpretation of colour in Figs. 9–16, the reader is referred to the web version of this article).

The contour maps of series "A" are shown in Fig. 9 and the bulk favorable green contour appears around the ester group suggesting that bulky groups around this region might be favorable for higher activity. This also can be seen with data that the compounds having bulky substituents around this region are highly active. The earlier study [4] also reports that site R1 is suitable for small group and R3 is most important site for bulkiness. CoMFA contour map of series "B" with electrostatic field effects has been shown in Fig. 10. A blue contour around R3 position above and below the plane indicates that a positive group around this site might have good effect. In earlier QSAR study of this series [4], the length of the substituents at position-3 was identified as most important factor for activity. Fig. 11 shows CoMFA contour map for series "C". The position R3 holds a bulk favorable green contour. Similarly, the position R1 holds yellow contour indicates that small group is desirable for better activity. In earlier study [4], the site R3 is identified to be important for bulk which supports our findings in a more visual and better way. Fig. 12 shows CoMFA map for series "D". The site R2 holds a blue contour, which indicates that positive group might have good effect on binding activity. The study by Litina et al. [4]

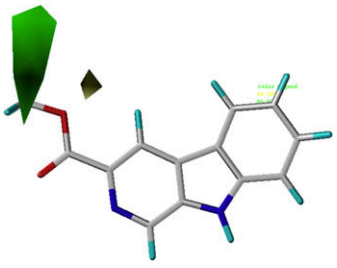

Fig. 9. The CoMFA map for series "A" of derivatives showing steric requirement for better activity.

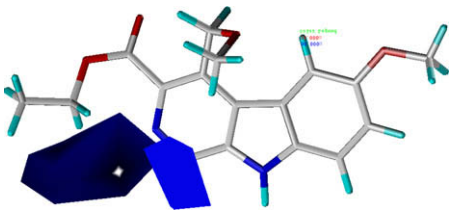

Fig. 10. The CoMFA map for series "B" of derivatives showing electrostatic requirement for better activity.

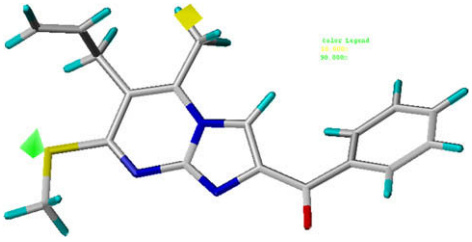

Fig. 11. The CoMFA map for series "C" of derivatives showing steric requirement for better activity.

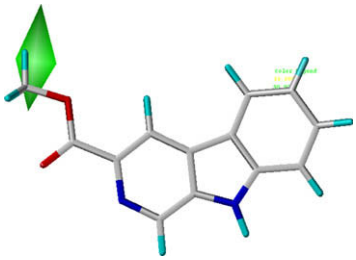

Fig. 13. Series "A" CoMSIA steric map.

was almost fail to identify either electrostatic or steric interaction for this series but Hollinshead et al. [16] proposed a possible electrostatic interaction from site R2 and the current study nicely supports to electrostatic interaction with site R2.

4.4. CoMSIA model

CoMSIA analyses were performed using steric, electrostatic and hydrophobic field effects as a descriptor. The procedure was almost same as for the CoMFA study and all three field descriptors were tested individually and in combination. In case of series "A", the steric field was most predictive which gives the value of $r^2 = 0.99$ with $r^2_{\text{predictive}} = 0.49$. Similarly in case of series "B", the value of q^2 for steric field is 0.68, for electrostatic field is 0.94, and for hydrophobic field is 0.21. In this case, the electrostatic field was most predictive which gives the value of $r^2 = 0.99$ with $r^2_{\text{predictive}} = 0.74$. The compounds of series "C" show strong relationship with steric field effects ($q^2 = 0.72$, $r^2 = 0.96$ with $r^2_{\text{predictive}} = 0.87$). These results are in agreement with CoMFA results. In case of series "D", the most significant model was based on hydrophobic field which gives the value of $q^2 = 0.47$, $r^2 = 0.72$ and $r^2_{\text{predictive}} = 0.60$. The predicted activities of training and test sets of compounds are reported in Tables 9–12 for series A–D, respectively. The statistical summary of different models is reported in Table 13.

4.5. The CoMSIA contour map

Figs. 13–16 show CoMSIA contour map of all four series with highly active molecules. On the basis of statistical quality of the results, steric field recognized important for the description of series "A".

In Fig. 13, the green contour favorable for bulk is located around the position R2. The experimental data are in consonance with the contour map as we can see all the active compounds have a bulky group at R2. Fig. 14 displays the CoMSIA contour map of series "B". The electrostatics field is most significant descriptor, the blue contour appears around position R1 indicates that a positively charged group might have good effect over activity. Fig. 15 shows the contour map of series "C", the green contour favorable for bulk is located around position R2 which indicates that a bulky group at this site might be helpful. The CoMSIA of series "D" was also made and the hydrophobic field effect was recognized as a best descriptor. In Fig. 16, a purple contour appears around the position R1 indicates that hydrophobic substituents are desirable around this site for better activity. Litina et al. [4] also suggested a possible hydrophobic interaction with site R1 and R2 but there was no clear indication for electrostatic interaction. The current study supports a combined electrostatic and hydrophobic interaction.

5. Discussion

The earlier study by Allen et al. [33] demonstrated that semi-empirical geometries and charges may be sufficient for making quantitatively useful predictions. Accordingly here, we have used semi-empirical geometries and charges in QSAR analyses. The study reveals that the steric field significantly contributes to binding affinity of series "A" and "C" but the electrostatic field nicely related with activity of series "B" and "D". To gain more insight, the CoMFA and CoMSIA were performed. The results are in agreement with physicochemical QSAR and 3D QSAR models were successfully validated with test set. A classical CoMFA analysis by Allen

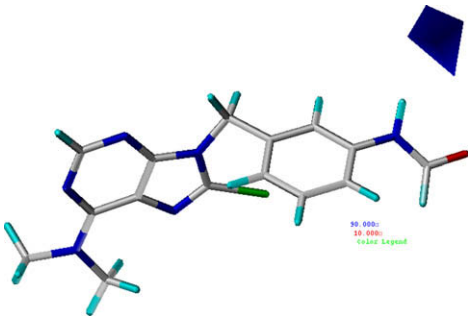

Fig. 12. The CoMFA map for series "D" of derivatives showing electrostatic requirement for better activity.

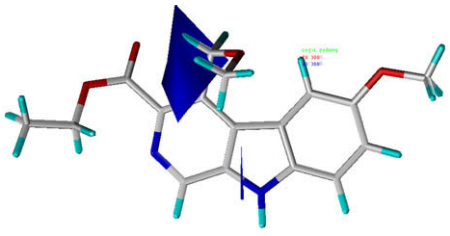

Fig. 14. Series "B" CoMSIA electrostatic map.

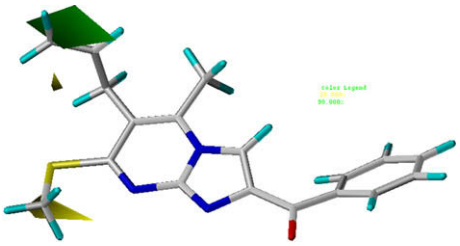

Fig. 15. Series "C", CoMSIA steric map.

et al. [13] describes significantly the structural requirement for β-Carbolines of series "A" by several other parameters rather than CoMFA alone which is probably due to diversity in data set. That study suggested that at site 3 a bulky group with hydrophobic effect might be helpful for better activity. The current study involved structurally similar 23 molecules, divided into 17 and 6 compounds of training and test sets, respectively. Physicochemical and 3D QSAR nicely relate the binding affinities with steric field effect and site R3 identified important for bulkiness as clear from Figs. 9 and 13. The earlier work by So et al. [11] related to similar compounds was based on electrostatic similarity index and nicely explains the QSAR but the data set contains heterogeneous compounds. The current study involves very similar compounds in data set which reveals that steric bulk is rather important than electrostatic interactions. The CoMFA of series "B" has been performed. The ligands were divided into training and test sets of 14 and 3 compounds, respectively. The 3D QSAR results are in agreement with physicochemical QSAR based results and the electrostatic field effect identified as a most important descriptor. An earlier work by Sharma et al. [14] reported the QSAR analysis of 10 compounds of same series and concluded that site 3 of β-Carolinas is important to hydrophobic interaction while the current study involves more number of molecules and explore the electrostatic aspects of interaction with a high statistics. In CoMFA of series "C", the data set was divided into training and test sets of 16 and 4 compounds, respectively. Physicochemical and 3D QSAR results reveal that steric field effects significantly contribute to binding affinities. Similarly in 3D QSAR of series "D", the data set was divided into training and test sets of 26 and 5 molecules, respectively. The physicochemical and 3D QSAR results reveal the dominance of electronic interactions with BzR. Recently Saha et al. [18] reported the QSAR of same data set by electronic parameters (σ and π values). The study focused on electronic properties only and nicely explains the QSAR with few outliers. The current study accounts the previous findings with high statistics with advanced approaches. The detailed study by Litina et al. [4]

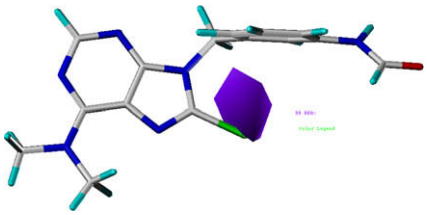

Fig. 16. Series "D" CoMSIA hydrophobic map.

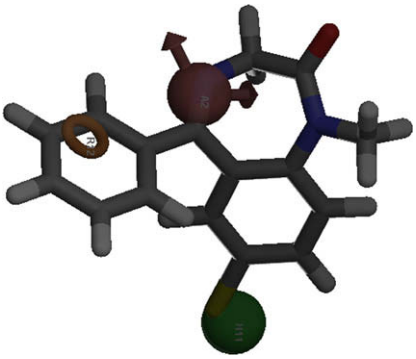

Fig. 17. The common pharmacophore perception in diazepam.

was successful but needs depth knowledge to identify the sites for further modifications. The results of current study support the assumptions of valuable contribution [4] and indicate similar interactions but the results are more visual and the important sites are identified by CoMFA and CoMSIA maps. It is difficult to give a statement regarding binding site due to lack of crystal structure of such ligands with receptor. But a recent docking result [34] with homology model showed that His102 is most important because of strong hydrogen-bonding interaction with benzo moiety of diazepam. Moreover, the residues Lys105, Tyr160, Tyr210 and Val212 in α1 subunit, and Phe77 in β2 subunit were all important ligand binding determinants as they had strong hydrophobic interaction. In case of diazepam, the three important pharmacophores (acceptor "A", hydrophobic "H" and ring "R") were identified and displayed in Fig. 17 by using Phase software. The hydrophobic and hydrogen bond acceptor sites were displayed by green and pink ball, respectively. The orange ring corresponds to aromatic center.

These three pharmacophores are common in all four series and the most active molecules of all four series were aligned by using these common pharmacophore and displayed in Fig. 18.

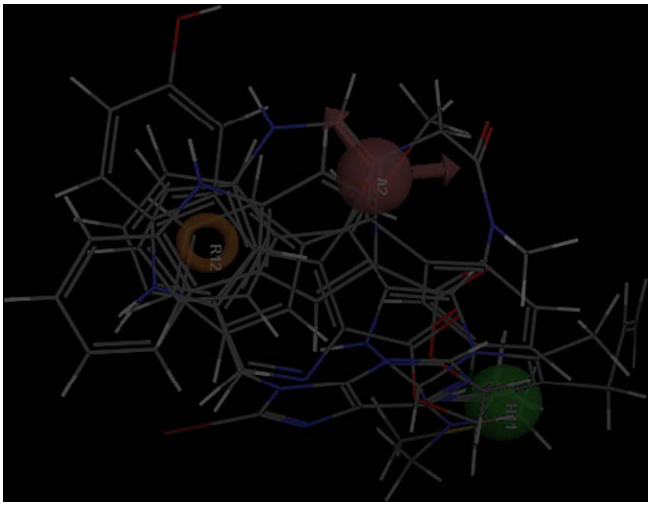

Fig. 18. The aligned structures of diazepam and most active molecules of four different series using common pharmacophore.

Table 14
The newly designed molecules of series A–D and their predicted activities by physicochemical QSAR, CoMFA and CoMSIA based models

Comp. no.	Series	R	R1	R2	R3	R4	PA_1	PA_2	PA_3	PA_{Avg}
1	A	–	H	$COOCBr(Me)_2$	–	–	7.33	8	8.51	7.95
2	A	–	H	$COOC(Br)_2Me$	–	–	7.01	8	8.7	7.9
3	A	–	H	$COOC(Br)_3$	–	–	9.28	8.2	8.2	8.56
4	B	OCH_3	CH_2OCH_3	H	$COOC_2H_5$	CCl_3	9.97	8.3	8.3	8.86
5	B	OCH_3	CH_2OCH_3	H	$COOC_2H_5$	CHO	10.15	9	8.2	9.12
6	B	OCH_3	CH_2OCH_3	H	$COOC_2H_5$	COOH	11.1	9.1	8.4	9.53
7	C	–	H	$CH_2CH{=}CH_2$	–	–	7.9	7.9	7.9	7.9
8	C	–	H	$CH_2CH{=}CCH_2$	–	–	7.75	7.8	7.5	7.68
9	C	–	H	$CH_2CH{=}CCH_2$	–	–	9.68	7.4	7.2	8.09
10	D	–	Br	$3\text{-}N(CF_3)CHO$	–	–	6.18	8.3	6.5	6.99
11	D	–	Br	$3\text{-}N(CHO)_2$	–	–	7.78	9.16	7.2	8.05
12	D	–	Br	3-N(CHO)COOH	–	–	6.89	9.1	6.65	7.55

The PA_1 = predicted activity by physicochemical QSAR based equations, PA_2 = predicted activities by CoMFA based best-fitted models, PA_3 = predicted activities by CoMSIA based best-fitted models and PA_{Avg} = average predicted activities.

The hydrophobic site, hydrogen-bonding site and an aromatic ring are present in all compounds of four series at almost same distance as in diazepam. This indicates that molecules might have same molecular interaction and binding mode within receptor as described for diazepam [34].

5.1. Design of new molecules based on QSAR models

The physicochemical, CoMFA and CoMSIA models described in the previous section were used to design some new molecules. The design strategy involved accordingly modifications in the substitution pattern of selected molecules from all four datasets. The possible candidate molecules (molecules 1–3 for series "A", 4–6 for series "B", 7–9 for series "C" and 10–12 for series "D") were reported in Table 14 with their predicted activities by three different QSAR models and the mean value of possible activities in reported binding essay conditions. The activities of the designed molecules are in better range. To sum up, the activity can be enhanced through suitable substitutions. Thus, the present QSAR models are powerful enough to suggest several fold improvement in the low affinity molecules. We hope that in the near future by using *in silico* modeling [35], our studies will enable us to design new effective drugs.

6. Conclusion

The study provides a better understanding of structural features with their binding affinities to BzR. All series (A–D) were studied [1–5,12–16,18] separately by different methods but the current study accounts three most important QSAR techniques (physicochemical QSAR, CoMFA and CoMSIA) together and these studies were indicated a similar interaction. The physicochemical study and 3D QSAR jointly suggested that the steric bulk interaction is dominant in series "A" and "C" and the electrostatic interaction is dominant in series "B" and "D". The log *P* and heat of formation were recognized as the best general descriptors for non-benzodiazepine derivatives. The CoMFA and CoMSIA models jointly suggested that, a bulky group is desirable on site R2 of series "A". In case of series "B", a positive group at pyridine ring might be helpful to improve the binding affinity. In case of series "C", a bulk at position R2 and small bulk at R3 might have good effect. Similarly for series "D", an electropositive group at R2 and a hydrophobic group at R1 might be helpful for better activity. In this way, the ligands of particular series may be designed for better performance. The study might be helpful to improve the biological activities of heterogeneous data set towards BzR.

Acknowledgment

The work is supported by KIST Linux supercomputer. We thank to Fujitsu for Cache evaluation version.

References

[1] T. Blair, G.A. Webb, Journal of Medicinal Chemistry 20 (9) (1977) 1206–1210.
[2] G. Greco, E. Novellino, C. Silipo, A. Vittoria, Quantitative Structure–Activity Relationships 11 (4) (1992) 461–477.
[3] S.P. Gupta, A. Paleti, Quantitative Structure–Activity Relationships 15 (1) (1996) 12–16.
[4] D. Hadjipavlou-Litina, R. Garg, C. Hansch, Chemical Reviews 104 (9) (2004) 3751–3793.
[5] S.P. Gupta, Progress in Drug Research 45 (1995) 67–106.
[6] R.D. Cramer, D.E. Patterson, J.D. Bunce, Journal of the American Chemical Society 110 (18) (1988) 5959–5967.
[7] F.A. Pasha, H.K. Srivastava, P.P. Singh, Bioorganic and Medicinal Chemistry 13 (24) (2005) 6823–6829.
[8] F.A. Pasha, K. Dal Nam, S.J. Cho, Molecular and Cellular Toxicology 3 (2) (2007) 145–149.
[9] P.P. Singh, F.A. Pasha, H.K. Srivastava, Indian Journal of Chemistry Section B – Organic Chemistry including Medicinal Chemistry 43 (5) (2004) 983–991.
[10] F.A. Pasha, H.W. Chung, S.J. Cho, S.B. Kang, International Journal of Quantum Chemistry 100 (2) (2000) 391–400.
[11] S.S. So, M. Karplus, Journal of Medicinal Chemistry 40 (26) (1997) 4360–4371.
[12] A.C. Good, S.J. Peterson, W.G. Richards, Journal of Medicinal Chemistry 36 (20) (1993) 2929–2937.

[13] M.S. Allen, Y.C. Tan, M.L. Trudell, K. Narayanan, L.R. Schindler, M.J. Martin, C. Schultz, T.J. Hagen, K.F. Koehler, P.W. Codding, P. Skolnick, J.M. Cook, Journal of Medicinal Chemistry 33 (9) (1990) 2343–2357.
[14] R.C. Sharma, T.N. Ojha, S. Tiwari, P. Singh, Drug Design and Discovery 9 (2) (1992) 135–143.
[15] M.S. Allen, T.J. Hagen, M.L. Trudell, P.W. Codding, P. Skolnick, J.M. Cook, Journal of Medicinal Chemistry 31 (9) (1988) 1854–1861.
[16] S.P. Hollinshead, M.L. Trudell, P. Skolnick, J.M. Cook, Journal of Medicinal Chemistry 33 (3) (1990) 1062–1069.
[17] S. Clements-Jewery, G. Danswan, C.R. Gardner, S.S. Matharu, R. Murdoch, W.R. Tully, R. Westwood, Journal of Medicinal Chemistry 31 (6) (1988) 1220–1226.
[18] R.N. Saha, J. Meera, N. Agrawal, S.P. Gupta, Drug Design and Delivery 7 (3) (1991) 219–226.
[19] J.L. Kelley, E.W. Mclean, R.M. Ferris, J.L. Howard, Journal of Medicinal Chemistry 32 (5) (1989) 1020–1024.
[20] J.L. Kelley, E.W. Mclean, J.A. Linn, M.P. Krochmal, R.M. Ferris, J.L. Howard, Journal of Medicinal Chemistry 33 (1) (1990) 196–202.
[21] A.K. Ghose, A. Pritchett, G.M. Crippen, Journal of Computational Chemistry 9 (1) (1988) 80–90.
[22] A. Klamt, G. Schuurmann, Journal of the Chemical Society – Perkin Transactions 2 (5) (1993) 799–805.
[23] R.G. Parr, R.G. Pearson, Journal of the American Chemical Society 105 (26) (1983) 7512–7516.
[24] R. Iczkowski, J.L. Margrave, Journal of the American Chemical Society 83 (17) (1961) 3547.
[25] R.G. Parr, L. Von Szentpaly, S.B. Liu, Journal of the American Chemical Society 121 (9) (1999) 1922–1924.
[26] M. Clark, R.D. Cramer, N. Vanopdenbosch, Journal of Computational Chemistry 10 (8) (1989) 982–1012.
[27] SYBYL 7.3, St. Louis, MO 63144, USA, 2007.
[28] G. Klebe, Perspectives in Drug Discovery and Design 12 (1998) 87–104.
[29] J.E. Lennard-Jones, Cohesion, Proceedings of the Physical Society 43 (1931) 461–482.
[30] G. Klebe, Journal of Molecular Biology 237 (2) (1994) 212–235.
[31] P. Geladi, Y.L. Xie, A. Polissar, P. Hopke, Journal of Chemometrics 2 (1998) 231.
[32] S. Wold, A. Ruhe, H. Wold, W.J. Dunn, SIAM Journal on Scientific and Statistical Computing 5 (3) (1984) 735–743.
[33] M.S. Allen, A.J. Laloggia, L.J. Dorn, M.J. Martin, G. Costantino, T.J. Hagen, K.F. Koehler, P. Skolnick, J.M. Cook, Journal of Medicinal Chemistry 35 (22) (1992) 4001–4010.
[34] S. Ci, T. Ren, Z. Su, The Protein Journal, in press.
[35] R.R.S. Pissurlenkar, M.S. Shaikh, E.C. Coutinho, Journal of Molecular Modeling 13 (10) (2007) 1047–1071.